BBA - Bioenergetics 1860 (2019) 111–120

Contents lists available at ScienceDirect

BBA - Bioenergetics

journal homepage: www.elsevier.com/locate/bbabio

# Energy transfer dynamics in a red-shifted violaxanthin-chlorophyll *a* light-harvesting complex

David Bína[a,c], Milan Durchan[b,c], Valentyna Kuznetsova[b], František Vácha[a,c], Radek Litvín[a,c], Tomáš Polívka[b,c,*]

[a] Institute of Chemistry, Faculty of Science, University of South Bohemia, Branišovská 1760, 37005 České Budějovice, Czech Republic
[b] Institute of Physics, Faculty of Science, University of South Bohemia, Branišovská 1760, 37005 České Budějovice, Czech Republic
[c] Institute of Plant Molecular Biology, Biological Centre, Czech Academy of Sciences, Branišovská 31, České Budějovice, Czech Republic

A B S T R A C T

Photosynthetic eukaryotes whose cells harbor plastids originating from secondary endosymbiosis of a red alga include species of major ecological and economic importance. Since utilization of solar energy relies on the efficient light-harvesting, one of the critical factors for the success of the red lineage in a range of environments is to be found in the adaptability of the light-harvesting machinery, formed by the proteins of the light-harvesting complex (LHC) family. A number of species are known to employ mainly a unique class of LHC containing red-shifted chlorophyll *a* (Chl a) forms absorbing above 690 nm. This appears to be an adaptation to shaded habitats. Here we present a detailed investigation of excitation energy flow in the red-shifted light-harvesting antenna of eustigmatophyte *Trachydiscus minutus* using time-resolved fluorescence and ultrafast transient absorption measurements. The main carotenoid in the complex is violaxanthin, hence this LHC is labeled the red-violaxanthin-Chl a protein, rVCP. Both the carotenoid-to-Chl a energy transfer and excitation dynamics within the Chl a manifold were studied and compared to the related antenna complex, VCP, that lacks the red-Chl a. Two spectrally defined carotenoid pools were identified in the red antenna, contributing to energy transfer to Chl a, mostly via $S_2$ and hot $S_1$ states. Also, Chl a triplet quenching by carotenoids is documented. Two separate pools of red-shifted Chl a were resolved, one is likely formed by excitonically coupled Chl a molecules. The structural implications of these observations are discussed.

## 1. Introduction

Although the rate of solar energy flux to Earth amounts to ~120,000 TW [1], sunlight is a diffuse energy source, in particular when molecular scales are considered: under full sunlight, only ~10 photons will be absorbed by a chlorophyll molecule per second [2] and this number will be significantly lower in most natural habitats. Hence, to sustain life-supporting energy input, all phototrophic organisms employ efficient energy-concentrating (light-harvesting) mechanisms.

In eukaryotic organisms, the light-harvesting machinery has typically the form of modular arrays of membrane proteins of the light-harvesting complex (LHC) family [3]. The structural motif of LHC proteins consists of three transmembrane helices that serve as a scaffold for binding pigment molecules (chlorophylls and carotenoids). Arguably the most primitive form of LHC system is found in extant red algae, where the LHCs serve the reaction center (RC) of photosystem I (PS I), whereas the phycobilisome, the light-harvesting antenna inherited from cyanobacteria, is mainly associated with photosystem II [4–6].

With the diversification of eukaryotic phototrophs, the family of LHC protein greatly expanded, replacing the phycobilisome entirely. This process was accompanied by diversification of pigment pools. While in red algae the LHC proteins bind only zeaxanthin and chlorophyll (Chl) a in 5 : 11–13 ratio per LHC monomer [7], LHC complexes of other eukaryotic phototrophs can accommodate also Chl b, several types of Chl c and a large variety of carotenoids, including carbonyl carotenoids [8]. These accessory pigments expand the spectral coverage of the antenna, effectively filling the energy gap between the $S_0$-$S_1$ (~670 nm) and $S_0$-$S_3$ (Soret, ~430 nm) absorption bands of Chl a. For example, the combination of carotenoids and Chl c found in many marine algae optimizes absorption properties of the light-harvesting apparatus for aquatic environment, where blue-green part is the most abundant [9].

A distinct strategy aiming at utilization of energies below that of the Chl a low energy band for oxygenic photosynthesis was first identified in cyanobacteria synthesizing unique red-shifted Chl d and Chl f [10,11]. This was interpreted as a response to adverse light conditions characterized by depletion of blue-green part of the solar spectrum and relative increase of the red component due to shading by other phototrophs that is encountered by species inhabiting biofilms and sediments in stratified aquatic environments [12] (see [13] for in situ spectra of light in various marine habitats).

More recently it became clear that light harvesting systems with

* Corresponding author: Institute of Physics and Biophysics, Faculty of Science, University of South Bohemia, Branišovská 1760, 370 05 České Budějovice, Czech Republic.
*E-mail address:* tpolivka@jcu.cz (T. Polívka).

https://doi.org/10.1016/j.bbabio.2018.11.006
Received 12 August 2018; Received in revised form 15 October 2018; Accepted 7 November 2018
Available online 08 November 2018
0005-2728/ 

absorption extending to the far red region, > 690 nm, are also present in a number of eukaryotic algae, including the green alga *Ostreobium* [14], and are broadly distributed especially among algae harboring chloroplast of red-algal origin: (pennate) diatoms, chromerids and eustigmatophytes [15–18]. Here, the expansion of the spectral coverage is not achieved by novel pigments but by modifying the properties of Chl a by pigment-pigment and pigment-protein interactions within unique types of LHC complexes [17–20]. Unifying features (apart from the red-shifted Chl a) shared by the known red LHCs are: i) oligomeric nature; the dissociation of oligomers is accompanied by the loss of the red-shifted Chl a forms; ii) preference for non-carbonyl carotenoids; this naturally includes eustigmatophytes that do not use carbonyl carotenoids in their LHCs but even in diatoms and chromerids that normally utilize fucoxanthins for light-harvesting, the red LHCs are depleted of these in favor of non-carbonyl diadinoxanthin and violaxanthin, respectively, compared to the main LHC complexes of these organisms [18–20].

So far, spectroscopic investigation of excitation energy transfer in these unique LHCs has been hampered by low stability of oligomeric preparations. This changed with the recent discovery of redLHCs in eustigmatophyte algae [18] shown to be considerably more stable in comparison to their diatom and chromerid counterparts.

Here we for the first time analyse in detail the excitation energy migration within a red-shifted antenna complex which represents the major antenna complex found in the freshwater eustigmatophyte *Trachydiscus minutus* (Goniochloridales, Heterokontophyta, [21,22]).

## 2. Material and methods

### 2.1. Sample preparation

The detailed description of *T. minutus* cell culture conditions and biochemical analysis of its antenna system will be presented elsewhere (Litvín et al. in preparation), a simplified description follows. The thylakoids were solubilized by n-dodecyl-β-D-maltoside (2% w/v) and fractionated on linear sucrose density gradient (0.1–1.1 M, 100,000 × g, 17 h). The green band with the highest $OD_{700}/OD_{674}$ ratio was collected, washed with sucrose-free isolation buffer (50 mM HEPES, pH 7.5, 2 mM KCl) and immediately loaded on Superdex 200 10/300 GL (GE Healthcare) size exclusion chromatography column to remove small amount of contaminating PSII RC complexes (see Supplementary Fig. S1). The most abundant antenna fraction with high $OD_{700}/OD_{674}$ was collected, mixed with glycerol (57% v/v) and frozen using OptistatDN2 cryostat (Oxford Instruments, Great Britain).

### 2.2. Spectroscopy

Steady-state absorbance spectra were measured using UV-1800 spectrophotometer (Shimadzu, Japan); fluorescence (excitation and emission) spectra were recorded using Fluorolog 3.2.2 (Horiba, Japan) spectrofluorometer, in perpendicular geometry.

Time-resolved fluorescence was measured using FluoTime 300 (PicoQuant, Germany) equipped with PMA-C-192 detector, using blue excitation source LDH-P-C-485; data were analyzed using the FluoFit (PicoQuant, Germany) software.

Ultrafast transient-absorption data were collected using femtosecond spectrometer based on a Ti:sapphire regenerative amplifier (Spitfire Ace−100F, Spectra-Physics, USA) seeded with a Ti:sapphire oscillator (MaiTai SP, Spectra-Physics, USA), and pumped by Nd:YLF laser (Empower 30, Spectra-Physics, USA). The laser system produces ~100 fs pulses centered at 800 nm with a 1-kHz repetition rate. Tunable excitation pulses were generated by an optical parametric amplifier (TOPAS Prime, Light Conversion, Lithuania). The probe pulses were generated by focusing a fraction of the 800 nm beam to a 2 mm sapphire plate to generate a broadband (450–750 nm) white light which was split by a broadband 50/50 beam splitter to a reference and probe beam. The probe beam was focused by a 300 mm spherical mirror to a sample where it overlaps with the excitation beam. Probe and reference beams were then focused to the entrance slit of a spectrograph where they were dispersed onto a double CCD array allowing measurements of transient spectra in a spectral window of ~250 nm. The time delay between the excitation and probe pulses was introduced by a computer-controlled delay line. The mutual polarization of the excitation and probe beams was set to the magic angle (54.7°) by placing a polarization rotator in the excitation beam. For all measurements, a 2-mm path length quartz cuvette was used. To avoid sample degradation, we employed a micro stirrer that continuously mixed the sample during the measurements.

Global analysis of the transient absorption data was performed using Glotaran software [24]. To visualize the excited state dynamics, we assumed sequential, irreversible scheme A → B, B → C, C → D… The arrows represent increasingly slower monoexponential processes and the time constants of these processes correspond to lifetimes of the species A, B, C, D… The spectral profiles of these species are called evolution-associated difference spectra (EADS), and although for complex systems they do not correspond to pure spectra of individual excited states, they provide valuable information about the time evolution of the whole system.

Steady-state absorbance and fluorescence measurements were performed in 1 × 1 cm PMMA cuvettes (Kartell, Italy); transient absorption measurements in 2 mm pathlength UVette cuvettes (Eppendorf, Germany).

### 2.3. Pigment analysis

Pigment composition of purified rVCP was analyzed using HPLC procedure described in [25] using ternary solvent system given in [26].

## 3. Results and discussion

### 3.1. Composition of the rVCP complex

In agreement with previous reports regarding the red-shifted antennas [17–19], the antenna complex from *T. minutus* investigated here is oligomeric. Comparison to PSII reaction center monomer [27] places its molecular mass to 300–400 kDa (Supplementary Fig. S1) based on the mass of PSII RC from [28]. Assuming LHC monomer mass of ~30 kDa this corresponds to an aggregate comprising > 10 LHC monomers.

Only violaxanthin (vio), non-esterified vaucheriaxanthin (vau) and Chl a were present in significant amounts in our antenna preparations (19 vio + 10 vau per 100 Chl a, see Fig. 1). Based on the pigment composition, we denote the red-shifted antenna from *T. minutus* rVCP (red-Violaxanthin-Chlorophyll Protein). In contrast to VCP of *Nannochloropsis*, where the ester accounted for 30% of total vau content [23], in rVCP we found only ~1 vau-ester per 100 Chl a. The pigment ratio of rVCP (3.4: 1 Chl a: car) corresponds more closely to 14 chlorophylls (a + b) and 4 carotenoids found in plant LHCII [29] than to VCP [23,30] where the Chl a-to-carotenoid ratio is ~2.

### 3.2. Steady state spectroscopy

In the Chl a $Q_y$ region, the absorbance spectrum of purified rVCP at 77 K has peaks at 667, 677 and 695 nm (Fig. 2). The carotenoid region shows a single peak at 487 nm with a minor shoulder around 500 nm. It is of interest to compare the spectral properties of rVCP complex to the "regular" VCP (black line in Fig. 2). The most conspicuous difference is found in the 650–690 nm window, namely presence of spectral features above 690 nm in rVCP. No such bands are observed in VCP although it does possess, in addition to the main $Q_y$ peak at 671 nm, a shoulder around 682 nm.

While the carotenoid region is qualitatively comparable in both

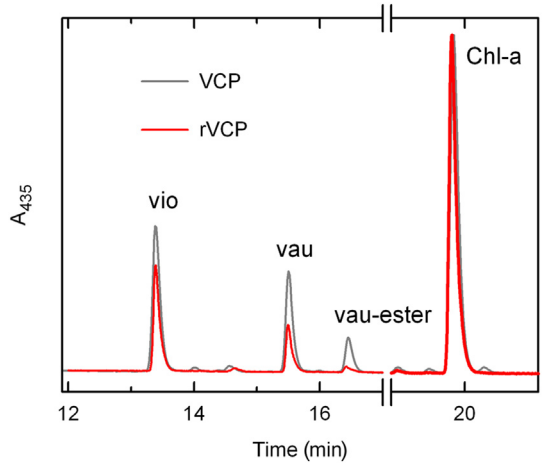


**Fig. 1.** Comparison of pigment composition of rVCP (red) and VCP. HPLC chromatogram detected at 435 nm; vio – violaxanthin; vau – vaucheriaxanthin; Chl-a – chlorophyll *a*.

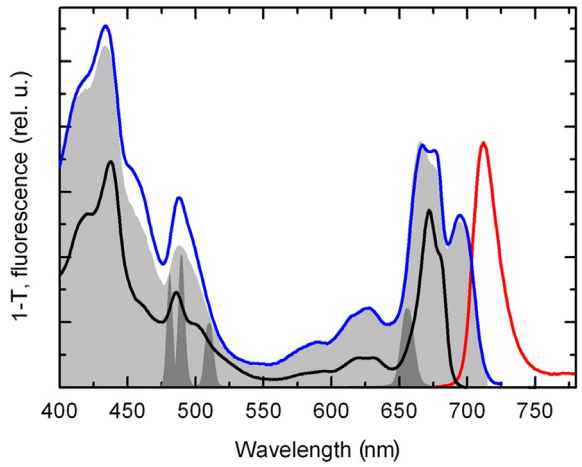


**Fig. 2.** Steady state absorption (blue) and fluorescence spectra of rVCP at 77 K; red line – emission spectrum; grey area – excitation spectrum for emission at 725 nm. The low temperature absorption spectrum of VCP complex from *N. oceanica* is also presented for comparison (black line). Small dark grey peaks show pump pulses used for fluorescence (481 nm) and transient absorption measurement (490, 510 and 656 nm).

complexes, certain differences can be found. In the rVCP complex, the carotenoid absorption does not extend beyond 520 nm, although in VCP a distinct band can be identified around 525 nm [31]. The shoulder around 500 nm, clearly visible in VCP, is also much less pronounced in rVCP. On the other hand, relative to the maximum of the Chl a Soret band, the intensity of the carotenoid bands in the 450–490 nm region is ~20% larger in rVCP. Since rVCP contains fewer carotenoids per Chl a than VCP, this means relative increase of the pool of blue-shifted carotenoids, at the expense of the red-shifted carotenoids.

Fluorescence emission spectrum of rVCP consists of a single peak with a maximum at 712 nm, as shown in Fig. 2 (excitation at 481 nm). The excitation spectrum (presented as the grey area in Fig. 2) detected at 725 nm shows energy transfer to the red Chl a forms, both from Chl a molecules absorbing at higher energy and from carotenoids. Yet, it shows that some carotenoids do not transfer energy to Chl a, yielding the overall efficiency of car-to-Chl a transfer ~80%.

Under closer inspection, there is a small discrepancy between the shape of the absorption and excitation spectra in the 677 nm band. This hints at a small proportion of Chl a absorbing around 670–680 nm not attached to the red forms, likely originating from dissociation of the complex. Comparison of the emission spectra excited at 435 nm (Chl a

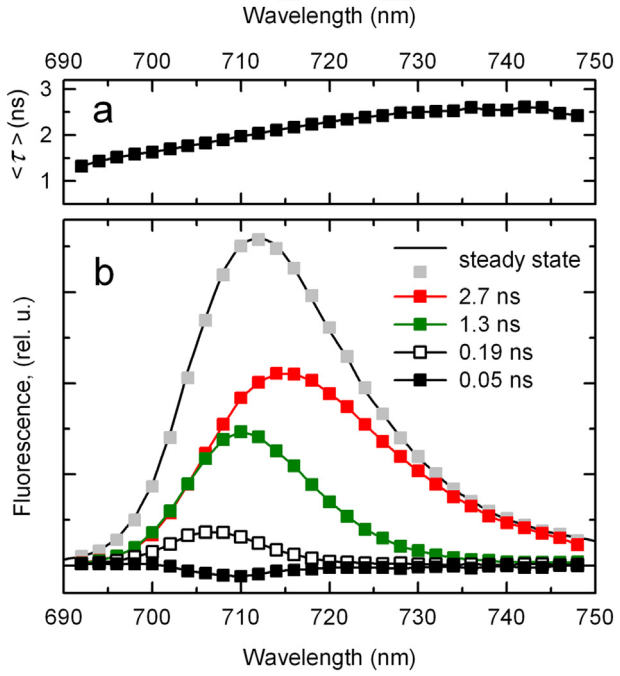


**Fig. 3.** Time-resolved fluorescence (TCSPC) data from rVCP at 77 K. (a) intensity-weighted average lifetime as a function of wavelength. (b) decay-associated spectra presented as intensities ($A \cdot \tau$). Black line represents the steady-state emission spectrum, grey squares denote the steady state spectrum computed from the DAS. Spectra were corrected for spectral sensitivity of the instrument.

Soret band) and into carotenoids at 481 nm (Supplementary Fig. S2) showed that direct Chl a excitation generated emission spectrum with slight broadening on the blue edge and a minor shoulder at ~680 nm, also indicative of 'free' Chl a contribution, whereas carotenoids excited at 480 nm were connected to the red-Chl a species, either directly or via other Chl a molecules.

### 3.3. Time-resolved fluorescence

Results from the time-resolved fluorescence measurement in the time window up to 20 ns are shown in Fig. 3. The average (intensity-weighted) fluorescence lifetime varied between 1.3 ns on the blue edge to 2.6 ns on the red edge of the emission band. This, ~1 ns variation is comparable to isolated LHCII trimers [32] but the LHCII lifetime at 77 K is about 2 times longer than rVCP. Also, the spectral development is considerably more complex in case of rVCP, requiring four components for adequate description: 50 ps, 190 ps, 1.3 ns and 2.7 ns, compared to 2 components of isolated detergent-solubilized LHCII [32]. The respective decay-associated spectra (DAS) are shown in panel b along with the steady state spectrum (identical to the red curve in Fig. 2). The dominant contribution to the characteristic red-shifted emission of the rVCP complex comes from the two slowest components peaking at 710 and 716 nm. The 190 ps component has significantly lower amplitude and peaks at 707 nm. The DAS of the fastest component is mostly negative (peaking at 710 nm) suggesting that it represents energy transfer process between spectral forms of Chl a. Given that the time bin of the present measurement was 25 ps, this fluorescence component is close to the time resolution limit and the lifetime can be assumed to carry a large error, however, ultrafast transient absorption data confirmed a 40 ± 10 ps component (see below).

The widths of the bands increased with increasing lifetime of the component by extending red-edge. The full width at half maximum (fwhm) of the four components corresponded to 200 $cm^{-1}$, 260 $cm^{-1}$, 330 $cm^{-1}$ and 490 $cm^{-1}$ going from 50 ps to 2.7 ns component. While

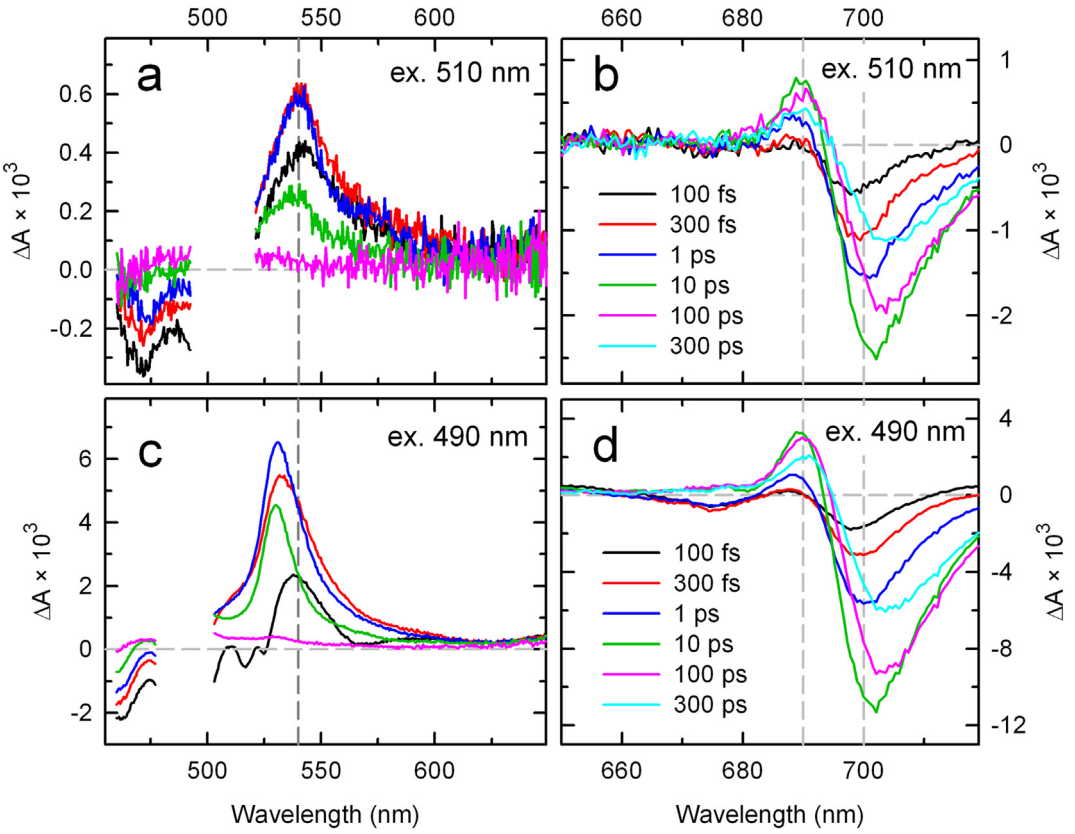


**Fig. 4.** Selected difference spectra in the carotenoid and Chl a $Q_y$ region of rVCP at 77 K following excitation into the carotenoid absorption band at 510 nm (a, b) and 490 nm (c, d). Vertical dashed line in panels (a) and (c) corresponding to 540 nm is shown to emphasize the difference in carotenoid excited state features following the two different excitations. Vertical lines in panels (b) and (d) are placed at 690 nm and 700 nm to facilitate appreciation of the spectral development.

values around 200 $cm^{-1}$ are comparable to Chl a in isolated LHCII trimers, much broader emission bands with expansion of the red tail have been taken as indicators of the charge-transfer character of the Chl a excited states. These have been observed in the oligomers of LHCa and LHCb proteins [33,34] and suggest a similar origin for the red-shifted Chl a states also in rVCP.

### 3.4. Transient absorption

For the time-resolved absorption we took advantage of the tunable excitation source and instead of 481 nm used for the fluorescence experiments, the excitation was set at 510 nm and 490 nm in an attempt to resolve different spectral pools of carotenoids, and at 656 nm to excite blue forms of Chl a to follow the energy flow within the Chl a pool. Fig. 4, showing transient absorption spectra after 490 and 510 nm excitations, clearly demonstrates existence of spectrally distinct carotenoids excited at each wavelength. There is a clear difference in position of the 0–1 band in the ground-state bleaching (GSB) of the carotenoid $S_0$-$S_2$ absorption band which has maxima at ~470 nm and ~460 nm for 510 and 490 nm excitations, respectively. A detailed spectral analysis of 77 K absorption spectrum shown in Supplementary Fig. S3 suggests that the corresponding positions of the 0–0 transition, obscured by the pump pulses in Fig. 4, are 499 nm and 488 nm, respectively. In the following, we will label the two carotenoid pools by the position of the pump pulse as the '510 nm' and '490 nm' pool.

#### 3.4.1. Carotenoid region

The spectroscopic difference between the two carotenoid pools is further reflected in the excited-state absorption (ESA) features (Fig. 4a, c), where about 10 nm difference of the position of maxima of the $S_1$-$S_N$ band was observed: 540 nm and 530 nm following excitation at 510 and 490 nm, respectively. Moreover, a closer look at the difference spectra immediately revealed differences in the excited state dynamics of the carotenoid pools: the amplitude of the carotenoid ESA band decreased by about 60% in the 510 nm carotenoid between 1 ps and 10 ps, whereas only 30% decrease was seen in the carotenoid excited at 490 nm. This is more clearly illustrated in Fig. 5a by comparing the traces taken at the maxima of $S_1$-$S_N$ ESA (540 and 530 nm). In this respect the observed behavior of the two carotenoid pools in rVCP corresponds to carotenoid dynamics reported for VCP [23].

#### 3.4.2. Chlorophyll a $Q_y$ region

Excitation at both 510 nm and 490 nm generated bleaching of a narrow Chl a absorption band peaking at ~698 nm on the timescale comparable to the duration of the pump pulse, signaling the presence of ultrafast energy transfer route from the $S_2$ state of both carotenoid pools. A shift of the Chl a bleaching maximum up to 705 nm, accompanied by broadening of the Chl a band followed, spanning the timescales from 0.1 to 100's ps. On the picosecond timescale (black datapoints and grey line in Fig. 5b), a conspicuous positive peak appeared at ~688 nm, by which the transient absorption spectrum of rVCP acquired the appearance typically associated with excitonically coupled bacteriochlorophylls in bacterial LH1 and LH2 antennas (e.g. [35,36]). As seen in Fig. 4 the zero crossing point shifted to the red with increasing the time delay after excitation (another parallel with the LH systems [36]).

The only major difference between the Chl a spectra for the two excitations can be identified in the region around 675 nm, where the excitation at 490 nm produced a weak bleaching signal that is absent after 510 nm excitation. This bleaching has the maximal amplitude (~50% of the 698 nm band) at 100 fs after 490 nm excitation. The 675 nm band decayed on the timescale of picoseconds.

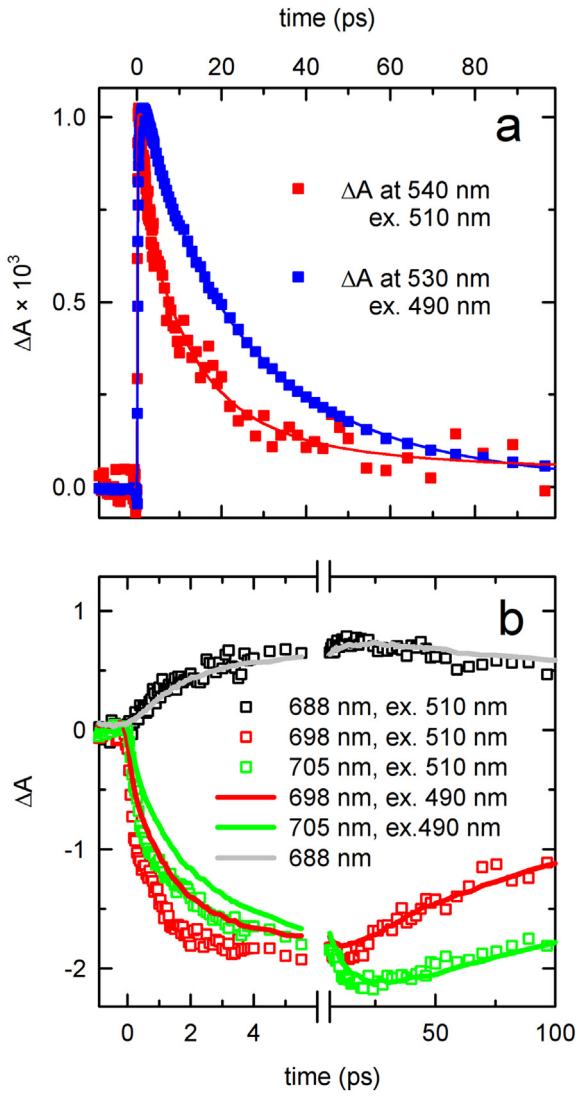


**Fig. 5.** Comparison of kinetics of selected absorption changes in rVCP at 77 K corresponding to carotenoids and Chl a following excitations into carotenoid absorption band. (a) kinetics at maximum of the carotenoid ESA. (b) kinetics of selected Chl a bands. Detection and excitation wavelengths are given in legend.

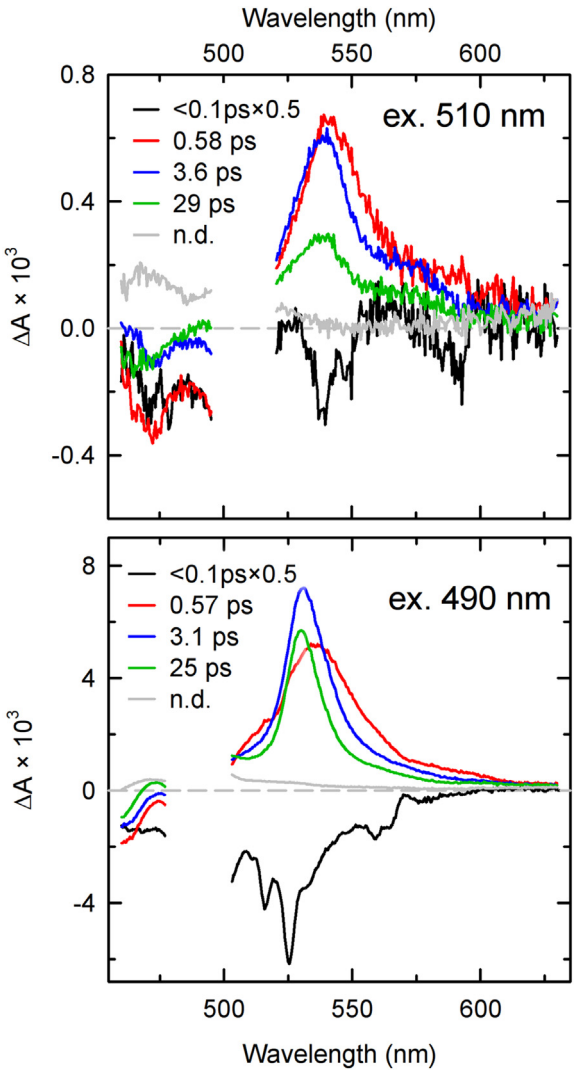


**Fig. 6.** Comparison of evolution associated spectra in the carotenoid region following excitation at 510 nm and 490 nm. Time constants corresponding to the shown EADS are given in legend.

Despite the similarity of the transient absorption spectra, dynamics of the Chl a states was different, as the rise of the Chl a bleaching was significantly faster following the excitation at 510 nm (Fig. 5b). A more detailed discussion of the dynamics of the Chl a excited states will be given later, but we will first focus on the analysis of processes within the carotenoid pools, representing the entry point for the excitation energy in the blue-green spectral region.

### *3.4.3. Dynamics of carotenoid excited states*

Since the evolution of the carotenoid excited states was completed in about 100 ps (Fig. 4) we limit the further analysis to this time window. The spectral region of interest was also limited to the region of the carotenoid bleaching and excited state absorption since it could be expected that the excited state dynamics observed in the Chl a region is, at least partially, independent of the energy transfer from carotenoids. Hence, including the $Q_y$ region could possibly complicate interpretation of the EADS resulting from overlapping carotenoid and Chl a dynamics, including e.g. relaxation within the Chl a excited states.

Results of the global fit of the carotenoid data using a sequential irreversible model are shown in Fig. 6. To interpret the EADS we will use comparison with VCP [23]. The first EADS, having a lifetime of < 100 fs, characterized by a negative signal covering the 450–600 nm range, can be assigned to the carotenoid $S_2$ state. The second EADS featured a broad band peaking at about 540 nm (ex. 510 nm) or 534 nm (ex. 490 nm), with a time constant ~0.6 ps. In the '510 nm' carotenoid pool, the decay of this EADS was accompanied by about 60% loss of the ground-state bleaching (GSB) at 470 nm, while less significant decay of GSB, about 25%, was associated with this decay component for the carotenoid excited at 490 nm. A straightforward assignment of this EADS feature would be the hot $S_1$, based on the red-shifted maximum and larger bandwidth compared to the relaxed $S_1$ state. For 490 nm excitation the second EADS has all attributes of the hot $S_1$ state. On the other hand, the EADS associated with the 0.58 ps component in the 510 nm excitation data has larger amplitude compared to the following EADS corresponding to relaxed $S_1$, which is unusual for the hot $S_1$ state [37,38]. However, considering the accompanying decrease of the $S_2$ GSB, the larger amplitude of the hot $S_1$ vs. $S_1$ EADS can be simply due to the overall decrease of the excited state population. The same issue was encountered previously in the VCP study [23] and resolved by interpreting the corresponding (0.33 ps in VCP at 300 K) component as an efficient energy transfer pathway from relaxed $S_1$ state for the carotenoid excited on the red edge of the spectrum (515 nm) rather than from a hot $S_1$ state. Regardless whether it is associated with hot or relaxed carotenoid $S_1$ state, this component

must be associated with energy transfer as its lifetime ~0.6 ps is significantly shorter than the corresponding lifetimes in organic solvent that yield for violaxanthin at 77 K 1.4 ps (hot $S_1$) and 33 ps ($S_1$) [37].

The identity of the donor state has however implications for the energy transfer rates from carotenoid to Chl a: if the donor state is the hot $S_1$ with intrinsic lifetime of ~1.4 ps, then the shortening to 0.6 ps corresponds to the transfer rate ~1 $ps^{-1}$ (~60% efficiency). On the other hand, since the lifetime of the relaxed carotenoid $S_1$ states is ~30 ps, the time constant for the transfer should be effectively identical to the measured lifetime of the donor state, i.e. ~0.6 ps, resulting in efficiency well over 95%.

The next, sharper ESA bands correspond to relaxed $S_1$ state with the lifetime of 3.1 and 3.6 ps in '490 nm' and '510 nm' carotenoid pool, respectively. The next EADS (green) corresponded also to $S_1$ state, but the lifetimes of 29 ps and 25 ps for the '510 nm' pool and '490 nm' pool, respectively, corresponds well to the $S_1$ lifetime at 77 K in organic solvent [37], indicating these carotenoids do not transfer energy to Chl a. This non-transferring component is dominant in the '490 nm' pool, while the 'fast' 3.6 ps component dominates after 510 nm excitation, mirroring the situation reported for VCP [23]. Thus, we invoke the interpretation suggested for the $S_1$ energy-transfer component in VCP from *N. oceanica* [23] that the carotenoid transferring from the $S_1$ state was excited preferentially at 510 nm, but small part of this pigment pool was also excited by the pump at 490 nm, leading to appearance of the minor 3–4 ps component.

### 3.4.4. Dynamics of Chl a excited states

EADS obtained from global fitting of the transient data in the Chl a $Q_y$ region are shown in Fig. 7. Compared to the carotenoid spectral region that yielded a rather straightforward interpretation, disentangling the evolution of the chlorophyll excited states represents a more difficult task in rVCP. The combined effect of energy transfer from carotenoids and energy transfer and relaxation within the Chl a excited state manifold lead to dynamic changes of amplitude, position and shape of the Chl a bleaching bands, making the separation of individual components complicated. This is very well illustrated in the first two EADS shown in Fig. 7 for both excitations. The first EADS represents the earliest Chl a state populated by transfer from $S_2$ state of carotenoids. The positive amplitude in the red tail of this EADS is most likely due to a high-energy edge of the ESA band pertinent to the $S_2 \rightarrow S_N$ transition [39,40]. However, the time constant assigned to this EADS clearly does not correspond to the lifetime of the $S_2$ state and, referring to the previous section, it does not correspond to expected transfer rate from any other carotenoid state. Hence, the ~230–250 fs process likely represents the relaxation of Chl a excited state (e.g. $Q_x$ populated from the carotenoid $S_2$ state) accompanied with the appearance of the stimulated emission [41,42], leading to the broadening on the red edge and a slight red-shift of the maximum of the negative band. The first EADS in Fig. 7b also shows that the excitation pathway initiated by excitation at 490 nm is split between the Chl a states at 675 nm and 698 nm.

The second EADS contains contribution from the negative band at ~675 nm. This feature is negligible (< 10% of the maximum bleaching at 700 nm) for the excitation at 510 nm, but represents ~30% of the amplitude of the main bleaching band after excitation at 490 nm. The time constant of the second EADS was ~1 ps for the excitation at 510 nm. For the excitation at 490 nm, this component is slower, 1.4 ps.

It is likely that the second EADS aggregates contribution from energy transfer from the carotenoid hot $S_1$ state (~0.6 ps) with energy transfer processes within the Chl a pool, since decay of this component is associated with a qualitative change of the Chl a difference spectrum, appearance of a positive band at 688 nm (observed in the third EADS). This feature remains present during the subsequent dynamic and can be explained as due to excitonic interaction between Chl a molecules based on similarity to the bacterial LH systems [35,36]. It can be concluded that these excitonically coupled Chl a molecules are not direct acceptors of the excitation energy from carotenoids as evidenced by a

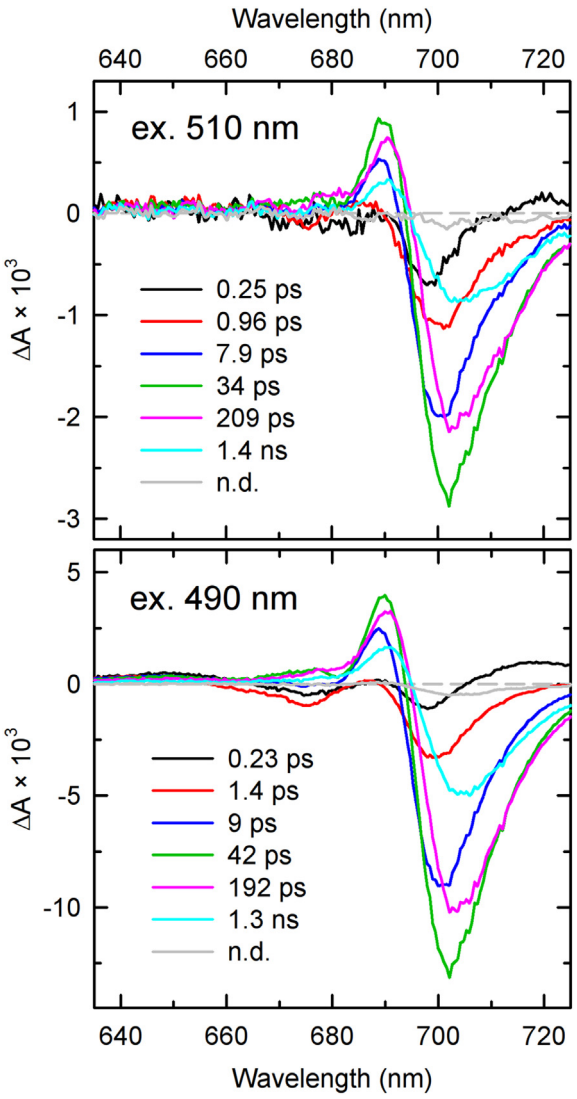


**Fig. 7.** Comparison of evolution associated spectra in the Chl a $Q_y$ region following excitation at 510 nm and 490 nm. Time constants corresponding to the shown EADS are given in legend.

significantly slower rise of the 688 nm signal compared to the bleaching at 698 nm following excitation of the carotenoids (Fig. 5b). However, the interpretation of the second EADS in the 490 nm excitation data is slightly more complex, because there is another contribution associated with energy transfer from Chl a at 675 nm, since this feature is absent in the third EADS.

The third EADS having lifetime of ~9 ps and ~8 ps when excited at 490 nm and 510 nm, respectively, is rather challenging to assign. This is the first component featuring prominent positive ESA band in the region 680–690 nm. While it is associated with increase of the Chl a bleaching, the time constant appears to be too long for energy transfer from carotenoid $S_1$ state (decaying in ~3–4 ps), hence it likely also contains a significant contribution of the energy transfer processes within the Chl a pool.

### 3.4.5. Decay of Chl a excited states, comparison to time-resolved fluorescence

The last three EADS in Fig. 7 span the time window from ~40 ps to several ns and describe the decay of the Chl a excited states. It should be noted that the respective time constants 34/42 ps, 209/192 ps and 1.4/1.3 ps for excitation at 510/490 nm are in very good correspondence to the lifetimes of fluorescence components shown in Fig. 3. This allows

for the assignment of the minor non-decaying EADS to the 2.7 ns component of fluorescence decay. Given that the energy of excitation pulse for the transient absorption measurements is ~0.2 μJ while it is about 10 pJ for the fluorescence experiment, observation of similar lifetime components suggests that nonlinear effects, such as singlet-singlet annihilation, are not the dominant factor responsible for the multiexponential decay of the Chl a excited states.

However, direct comparison of the decay traces (Supplementary Fig. S4) reveals difference in relative contributions of the individual decay components in the time resolved absorption and fluorescence. The decay in transient absorption is clearly dominated by the faster components leading to a significantly shorter average lifetime of Chl a excited states. The 30–40 ps component in the transient absorption data is clearly associated with a decrease of the Chl a bleaching (Fig. 7), in addition to the red-shift of the absorption band. In contrast, the 50 ps component in the time-resolved fluorescence (Fig. 3) has negative amplitude indicating that it represents an energy transfer rather than decay step.

Altogether, this leads to a conclusion that even at pulse energies significantly under 1 μJ, the transient absorption experiment was not performed at fully annihilation-free conditions, and that contribution of singlet-singlet annihilation is observed in the 30–40 ps component of the Chl a dynamics. This is not surprising, considering the estimated size of the complex and its pigment content: an rVCP oligomer corresponds to a pool of over 100 Chl a molecules and 40 carotenoids (see Section 3.1.), which makes it in this respect comparable to e.g. PSI which requires pulse energies on the order of a few nJ to avoid annihilation [43]. Presence of singlet-singlet annihilation in rVCP also indicates excitation energy migration over the antenna oligomer.

The presence of annihilation in transient absorption notwithstanding, the time-resolved data clearly show that the decay of the Chl a excited states is multiexponential. Components on the order of 10–100 ps were previously observed in Lhca and interpreted as pigment-protein relaxation [44], however, whether this can be applied to glass-embedded system at 77 K is questionable. A more recent study [45] indicated that Lhca4 complex, which also harbors red-shifted Chl a, exists in several conformations, presumably related to light-harvesting and quenching forms of the complex. It should be noted that the red-most component with the longest lifetime ~2.5 ns, and the shorter-lived components corresponding to higher-energy Chl a species decaying on 100 ps to ns timescales are shared by Lhca4 and rVCP, although comparisons of rVCP to other systems have to be taken with caution, given the limited knowledge of the molecular details of the algal complex. On the other hand, the ability of rVCP to switch between light-harvesting and quenching forms in rVCP would be in line with observations of nonphotochemical quenching in *T. minutus* [46].

### 3.4.6. Direct $Q_y$ excitation

To deepen the insight into the dynamics of the Chl a excited states we applied also excitation at 656 nm. As seen from Fig. 2, at this wavelength the energy transfer efficiency to the red-Chl a states is nearly 100%, comparable to the excitation to the red-edge of the carotenoid band at 510 nm.

The corresponding transient absorption spectra and EADS are shown in Fig. 8. It is obvious that the temporal development of the spectra is similar to that obtained after excitation of carotenoids, especially the '490 nm' pool. Yet, direct Chl a excitation at 656 nm generates an extra bleaching band at ~660 nm that is absent in the carotenoid-excited spectra. The negative band at 675 nm observed after excitation of the '490 nm' carotenoid pool is present also in the data shown in Fig. 8.

The complex dynamics related to relaxation within the Chl a pool in rVCP required eight components to fit the data obtained after the direct $Q_y$ excitation. The first EADS, < 100 fs, corresponds to relaxation of the initially excited state leading to population of the 675 nm and 697 nm Chl a states. The second, ~800 fs, component is associated with the

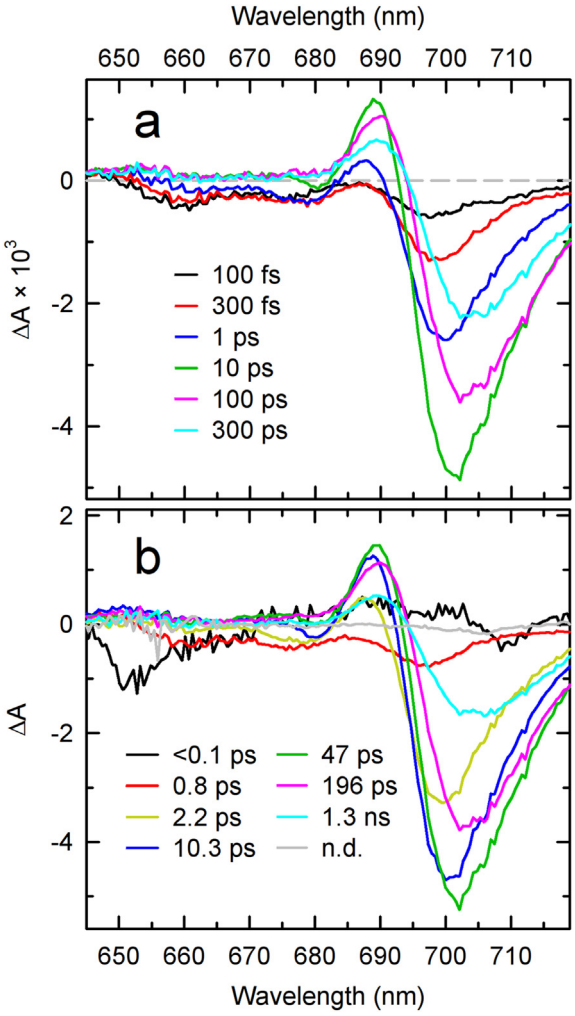


**Fig. 8.** Results of excitation of rVCP at 656 nm. (a) difference absorption spectra in the Chl a absorption region at selected time intervals. (b) EADS with corresponding time constants.

decay of the 660 nm band accompanied with the increase of bleaching at 700 nm. The decay of the second EADS is associated with the development of the ESA signal around 688 nm, as in the case of carotenoid excitation discussed in previous sections. Furthermore, the second step is accompanied by ~2 fold increase of the total Chl a bleaching, estimated from the area of the negative signal over the range 650–730 nm. This may indicate exciton interaction in a manner similar to bacterial LH2 complexes, where energy transfer from monomeric B800 bacteriochlorophyll to excitonically coupled B850 pigments is also accompanied by a large increase of bleaching amplitude [35]. This is also in agreement with interpretation of the positive 688 nm ESA band as the transition between the exciton levels.

The next, ~2.2 ps component pertains to the decay of the 675 nm band and further development of the 688 nm ESA band. The 2.2 ps component is followed by an EADS characterized by a positive maximum at ~690 nm and negative peak at 700 nm having a time constant of ~10 ps. The overall shape of this feature as well as the time-constant suggest that it corresponds to the 8–9 ps component observed following excitation into carotenoids and thus represent the species to which all the excitation transfer paths in the rVCP complex converge. This is further supported by the striking similarity of the 'slow' EADS extracted from data measured after different excitations (Supplementary Fig. S5).

### 3.4.7. The 'high-energy' Chl a states

Final aspect of the excited state dynamics is the contribution of the

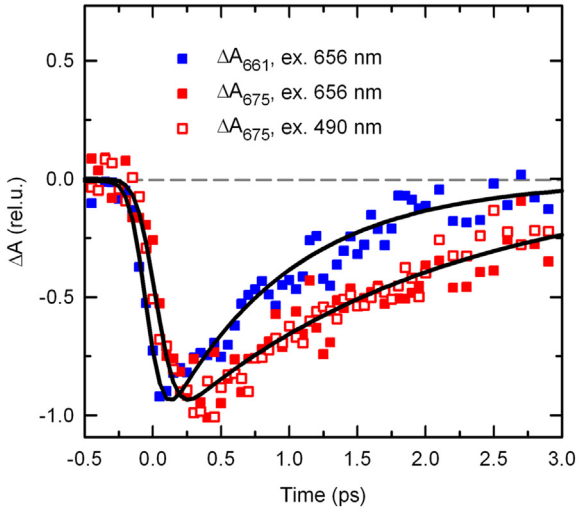


**Fig. 9.** Comparison of kinetics of absorbance corresponding to the high-energy Chl a species (661 and 675 nm) following carotenoid and Chl a excitation, as shown in legend.

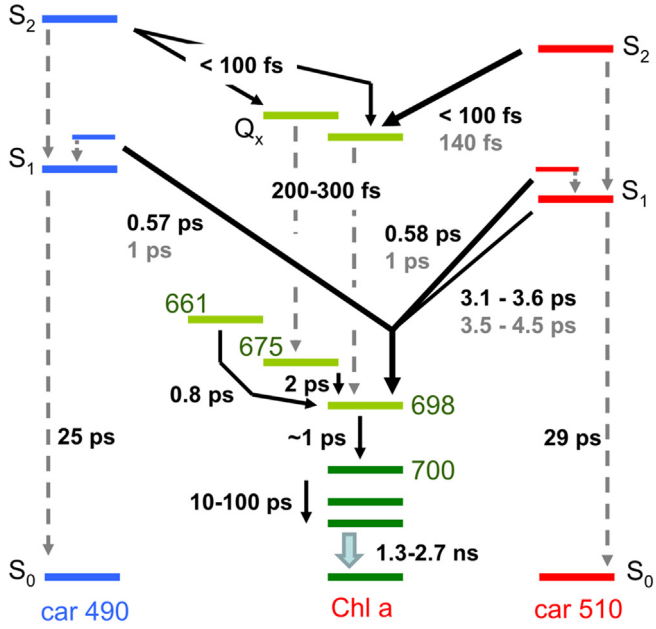


**Fig. 10.** Scheme of excitation energy transfer pathways in the rVCP complex at 77 K. Observed time constants are shown in black. Grey numbers show the time constants of the carotenoid-Chl a energy transfer steps computed using lifetimes of carotenoid excited states in solution at cryogenic temperatures taken from [37]. Position of the maxima of the Chl a bands involved in the earliest energy transfer steps are shown. The 1.3–2.7 ns value corresponds to the observed fluorescence lifetime of the two slowest Chl a components from the fluorescence lifetime experiment. The dark green colour indicates the excitonically coupled Chl a states.

Chl a species absorbing at wavelengths shorter than 680 nm. As shown by comparison of direct Chl a (656 nm) and carotenoid (490 and 510 nm) excitation, the Chl a absorbing at 660 nm do not participate in the energy transfer from carotenoids, paralleling the situation of the high-energy Chl a in VCP [23]. Kinetic trace at 661 nm is in Fig. 9 compared to the kinetics at 675 nm for both the excitation at 656 nm and 490 nm. It is notable that the maxima of the kinetics at 661 nm and 675 nm occur no more than 200 fs apart (Fig. 9). Considering the observed lifetime of the 661 nm state of ~1 ps, the data shown in Fig. 9 demonstrate that the energy transfer from the 661 nm state towards the lower energy Chl a acceptor (690–700 nm) does not involve participation of the Chl a 675 nm.

### 3.4.8. Summary of pathways of singlet excitation energy transfer in rVCP

Analysis of the initial steps of the (singlet) energy transfer pathways in rVCP presented in the previous paragraphs can be summarized as follows (see Fig. 10): i) two pools of carotenoids can be distinguished, with corresponding position of the 0–0 bands of the $S_0$-$S_2$ transition at 488 and 499 nm; ii) $S_2$ and hot $S_1$ appear to be the dominant energy donors to Chl a, with observed lifetimes of < 100 fs and ~0.6 ps, respectively, for both carotenoid pools. However, it should be noted that there are two $S_2$ pathways initiated by the 490 nm excitation, one going directly to the Chl a at 698 nm, the other involving the intermediate 675 nm Chl a species which then transfers to Chl a 698 on picosecond timescale; iii) carotenoid molecules donating excitation from the relaxed $S_1$ state are present, although this pathway is of minor importance and has relevant contribution only for the carotenoids excited at 510 nm. The respective decay rate was found to be $(3–4\ ps)^{-1}$. The decay rate of the $S_1$ state of the non-transferring carotenoid is 25–29 ps which is in reasonable agreement with the value reported in frozen solution (33.5 ps [37]). Overall, excited state dynamics in the rVCP complex is remarkably similar to its non-red-shifted counterpart, VCP from *N. oceanica*. The lifetime of the hot $S_1$ excited state is longer in rVCP than VCP (~0.3 ps), however, considering about 2 fold prolongation of the lifetime of the hot $S_1$ at 77 K [37], it can be concluded that the efficiency of the energy transfer from this state is in fact also comparable in the two antenna complexes. In Fig. 10 we give the observed lifetimes of the excited states as well as the estimated rate constants for the energy transfer steps (grey) computed using the published lifetimes of violaxanthin excited states in solution at 77 K [37], $S_2 \rightarrow$ hot $S_1$, 0.19 ps, hot $S_1 \rightarrow S_1$,1.4 ps. Using these values one can for the simpler case of the 510 nm excitation derive a rough estimate of the contribution of the carotenoid states to the overall energy transfer of $S_2$: 57% hot $S_1$: 25%, $S_1$: 16%, resulting in total efficiency of 98%, which is a reasonable estimate for the red edge of the carotenoid absorption band in rVCP.

The initial spectral evolution of the $Q_y$ region was dominated by features related to the Chl a excited states dynamics, with the time constants of 200–300 fs, ~1 ps and 8–10 ps. We assigned these to relaxation of the Chl a excited state ($Q_x \rightarrow Q_y$), followed by two energy transfer steps within the red Chl a pool, transferring energy from the initial acceptor state at 698 nm on a picosecond timescale.

### 3.5. Triplet states

Previous paragraphs showed that in terms of the carotenoid-to-Chl a energy transfer properties, the rVCP does not differ significantly from the regular VCP lacking the red Chl a forms. At this point, one issue of the interaction of Chl a with carotenoids remains unresolved: quenching of Chl a triplet states. It is known that all LHCs are efficiently protected against Chl a triplet states by carotenoids, independently of the composition of the carotenoid pool bound in the complex. The time constant of the triplet transfer from Chl a to carotenoid are likely on the order of 100 ps or even shorter [47], so no accumulation of Chl a triplet occurs and the carotenoid triplet state appears to be populated with the kinetics of the Chl a excited state decay [48]. As shown in the Supplementary Fig. S6, the same applies to *N. oceanica* VCP at 77 K, where the kinetics of the carotenoid triplet formation matches the Chl a excited singlet state, decaying monoexponentially with 3.9 ns lifetime.

The rVCP offered a different picture in the ultrafast experiment. Here, the carotenoid triplet yield was much lower and a major part of the decay of the red Chl a excited state was not accompanied with a carotenoid triplet rise. Referring back to the comparison of transient absorption and fluorescence measurements (see Section 3.4.5.), the likely reason for this are nonlinear effects, such as singlet-singlet annihilation occurring in rVCP, depleting the Chl a excited state.

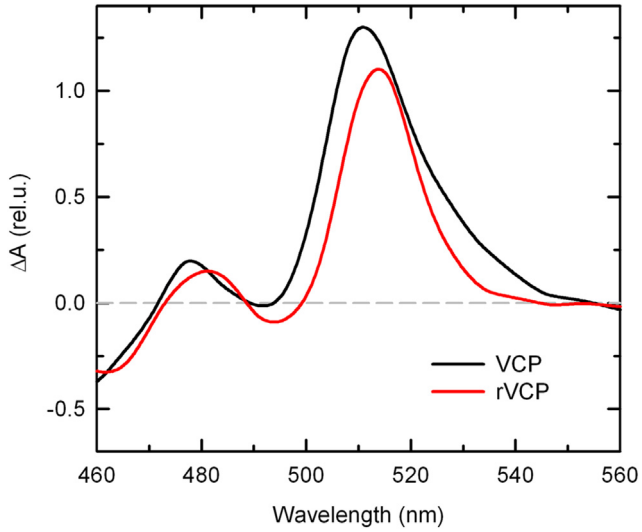


**Fig. 11.** Triplet-minus-singlet difference absorption spectra of rVCP (red) and VCP (black) at 77 K measured at time delay 5 μs following 1.5 μs broadband actinic pulse from xenon-flash lamp. The samples were excited through a 600 nm cut-off long-pass filter and the difference spectra were normalized to the integral of the $Q_y$ region of steady state 1-T spectra of the samples.

However, an important conclusion can still be derived from the data. The time constant of the carotenoid triplet rise could only be roughly estimated but it must be clearly in the ns range, implying that the carotenoid triplets are populated from triplets of the red-shifted Chl a species in rVCP.

To overcome, at least partially, the nonlinear effects and allow for a better comparison of the triplet yield in rVCP and VCP, the triplet-minus-singlet spectra were measured using microsecond flash-photolysis using xenon flash lamps as the exciting light source. In this case, the energy of individual pulses is in the 100 μJ range. However, since this is delivered over the 1.5 μs duration of the pulse, the probability of the singlet-singlet annihilation is much lower than in the femtosecond experiment, while the triplet states are still efficiently produced. Comparison of the triplet-minus-singlet spectra in the carotenoid region measured in the microsecond regime is shown in Fig. 11. The samples were adjusted to the same OD at $Q_y$ maximum as for the ultrafast experiments and excited through 600 nm long-pass filter. The resulting spectra were scaled to the integral of the steady state absorption spectrum (1-T) of the complexes in the 600 nm–750 nm region. These measurements showed that yield of carotenoid triplet in the rVCP complex is most likely comparable to the VCP and thus presence of the red Chl a forms does not affect negatively the triplet quenching function.

## 4. Conclusions

While the lack of the protein sequences complicates derivation of conclusion regarding the relation between function and structure in rVCP, there is no doubt that rVCP is a member of the LHC family and this implies presence of the conserved core of two carotenoids in close contact with three Chl a (e.g [49]).

Present results suggest existence of two different pools of red-shifted Chl a, differing by their spectral signatures in rVCP. The first group, lacking significant ESA bands in the $Q_y$ region, participates in the energy transfer from carotenoids. This indicates that these Chl a molecules should be located in the core of the LHC complex. The dynamics of the carotenoid excited states in the rVCP correspond very well to the regular VCP complex lacking the red-shifted Chl a, suggesting that the presence of these low-energy chlorophyll forms | does not significantly affect the pigment organization in the LHC core region.

The second group of Chl a molecules, absorbing at 700 nm and above, featuring prominent ESA bands, which are reminiscent of those known for excitonically coupled bacteriochlorophylls in purple bacterial antenna [35,36], does not participate directly in carotenoid-Chl singlet energy transfer, and most likely involves peripherally positioned Chl a, e.g. molecules situated between the subunits of the antenna oligomer. This agrees with high Chl a : carotenoid ratio of the red-shifted antenna compared to VCP, indicating presence of additional Chl a molecules in rVCP.

On other hand, we also demonstrate that the lowest-energy Chl a forms are protected by carotenoids against triplet states. Considering that the triplet transfer proceeds via a Dexter exchange mechanism requiring an overlap between electron orbitals of the donor and acceptor, the photoprotective carotenoid has to be also located in the vicinity of the red chlorophylls, hence on the periphery of the complex.

As judged from the broadened emission bands, red Chl a states decaying on the ns scale, they appear to possess a degree of charge transfer, although confirmation of this assertion would require further experiments, such as Stark spectroscopy. While Chl CT states have been implicated in the excitation energy quenching in aggregated light-harvesting complexes [33], in the case of rVCP they clearly serve the light harvesting function. In fact, it is known that nonphotochemical processes in *T. minutus* are the same as in the related algae lacking red-shifted Chl a forms [46], hence the presence of red-shifted Chl a CT states is not sufficient for the quenching function of the LHC [44,50].

In this respect the red-shifted algal LHC might represent a very useful model system for the investigation of structural and functional requirements for regulation of light-harvesting and photoprotective functions in eukaryotic light-harvesting complexes in addition to its inherent interest as a unique biophysical mechanism of ecological adaptation.

## Transparency document

The Transparency document associated with this article can be found, in online version.

## Acknowledgments

The research was funded from the Czech Science Foundation grant P501/12/G055, and by institutional support RVO:60077344.

## Appendix A. Supplementary data

Supplementary data to this article can be found online at https://doi.org/10.1016/j.bbabio.2018.11.006.

## References

[1] R.E. Blankenship, D.M. Tiede, J. Barber, G.W. Brudvig, G. Fleming, M. Ghirardi, M.R. Gunner, W. Junge, D.M. Kramer, A. Melis, T.A. Moore, C.C. Moser, D.G. Nocera, A.J. Nozik, D.R. Ort, W.W. Parson, R.C. Prince, R.T. Sayre, Comparing photosynthetic and photovoltaic efficiencies and recognizing the potential for improvement, Science 332 (2011) 805–809.
[2] R.E. Blankenship, Molecular Mechanisms of Photosynthesis, Blackwell Science, Oxford, UK, 2014.
[3] B.R. Green, D.G. Durnford, The chlorophyll-carotenoid proteins of oxygenic photosynthesis, Annu. Rev. Plant Physiol. Plant Mol. Biol. 47 (1996) 685–714.
[4] F.X. Cunningham, R.J. Dennenberg, P.A. Jursinic, E. Gantt, Growth under red light enhances photosystem II relative to photosystem I and phycobilisomes in the red alga *Porphyridium cruentum*, Plant Physiol. 93 (1990) 888–895.
[5] G.R. Wolfe, F.X. Cunningham, D.G. Durnford, B.R. Green, E. Gantt, Evidence for a common origin of chloroplasts with light harvesting complexes of different pigmentation, Nature 367 (1994) 566–568.
[6] J. Marquardt, E. Rhiel, The membrane-intrinsic light-harvesting complex of the red alga *Galdieria sulphuraria* (formerly *Cyanidium caldarium*): biochemical and immunochemical characterization, Biochim. Biophys. Acta 1320 (1997) 153–164.
[7] X. Pi, L. Tian, H.-E. Dai, X. Qin, L. Cheng, T. Kuang, S.-F. Sui, J.-R. Shen, Unique organization of photosystem I–light-harvesting supercomplex revealed by cryo-EM from a red alga, Proc. Natl. Acad. Sci. U. S. A. (2018), https://doi.org/10.1073/pnas.1722482115 (in press).

[8] A.W.D. Larkum, Light-harvesting systems in algae, in: A.W.D. Larkum, S.E. Douglas, J.A. Raven (Eds.), Photosynthesis in Algae, Springer, Netherlands, 2003, pp. 277–304.
[9] R.E. Blankenship, M. Chen, Spectral expansion and antenna reduction can enhance photosynthesis for energy production, Curr. Opin. Chem. Biol. 17 (2013) 457–461.
[10] H. Miyashita, H. Ikemoto, N. Kurano, K. Adachi, M. Chihara, S. Miyachi, Chlorophyll d as a major pigment, Nature 383 (1996) 402.
[11] M. Chen, Y. Li, D. Birch, R.D. Willows, A cyanobacterium that contains chlorophyll f—a red-absorbing photopigment, FEBS Lett. 586 (2012) 3249–3254.
[12] M. Kühn, M. Chen, P.J. Ralph, U. Schreiber, A.W.D. Larkum, A niche for cyanobacteria containing chlorophyll d, Nature 433 (2005) 820.
[13] B. Sundarabalan, P. Shanmugam, Modelling of underwater light fields in turbid and eutrophic waters: application and validation with experimental data, Ocean Sci. 11 (2015) 33–52.
[14] B. Koehne, G. Elli, R.C. Jennings, C. Wilhelm, H. Trissl, Spectroscopic and molecular characterization of a long wavelength absorbing antenna of *Ostreobium* sp, Biochim. Biophys. Acta 1412 (1999) 94–107.
[15] Y. Fujita, K. Ohki, On the 710 nm fluorescence emitted by the diatom *Phaeodactylum tricornutum* at room temperature, Plant Cell Physiol. 45 (2004) 392–397.
[16] E. Kotabová, J. Jarešová, R. Kaňa, R. Sobotka, D. Bína, O. Prášil, Novel type of red-shifted chlorophyll a antenna complex from *Chromera velia*. I. Physiological relevance and functional connection to photosystems, Biochim. Biophys. Acta 1837 (2014) 734–743.
[17] M. Herbstová, D. Bína, P. Koník, Z. Gardian, F. Vácha, R. Litvín, Molecular basis of chromatic adaptation in pennate diatom *Phaeodactylum tricornutum*, Biochim. Biophys. Acta 1847 (2015) 534–543.
[18] B.M. Wolf, D.M. Niedzwiedzki, N.C.M. Magdaong, R. Roth, U. Goodenough, R.E. Blankenship, Characterization of a newly isolated freshwater Eustigmatophyte alga capable of utilizing far-red light as its sole light source, Photosynth. Res. 135 (2018) 177–189.
[19] D. Bína, Z. Gardian, M. Herbstová, E. Kotabová, P. Koník, R. Litvín, O. Prášil, J. Tichý, F. Vácha, Novel type of red-shifted chlorophyll a antenna complex from *Chromera velia* II. Biochemistry and spectroscopy, Biochim. Biophys. Acta 1837 (2014) 802–810.
[20] M. Herbstová, D. Bína, R. Kaňa, F. Vácha, R. Litvín, Red-light phenotype in a marine diatom involves a specialized oligomeric red-shifted antenna and altered cell morphology, Sci. Rep. 7 (2017) 11976.
[21] P. Přibyl, M. Eliáš, V. Cepák, J. Lukavský, P. Kaštánek, Zoosporogenesis, morphology, ultrastructure, pigment composition, and phylogenetic position of *Trachydiscus minutus* (Eustigmatophyceae, Heterokontophyta), J. Phycol. 48 (2012) 231–242.
[22] K. Fawley, M. Eliáš and M. Fawley, The diversity and phylogeny of the commercially important algal class Eustigmatophyceae, including the new clade Goniochloridales, J. Appl. Phycol. 26 (2914) 1773–1782.
[23] G. Keşan, R. Litvín, D. Bína, M. Durchan, V. Šlouf, T. Polívka, Efficient light-harvesting using non-carbonyl carotenoids: energy transfer dynamics in the VCP complex from *Nannochloropsis oceanica*, Biochim. Biophys. Acta 1857 (2016) 370–379.
[24] J.J. Snellenburg, S.P. Laptenok, R. Seger, K.M. Mullen, I.H.M. van Stokkum, Glotaran: a Java-based graphical user interface for the R package TIMP, J. Stat. Softw. 49 (2012) 1–22.
[25] R. Litvín, D. Bína, M. Herbstová, Z. Gardian, Architecture of the light-harvesting apparatus of the eustigmatophyte alga *Nannochloropsis oceanica*, Photosynth. Res. 130 (2016) 137–150.
[26] S. Jeffrey, R. Mantoura, S. Wright, Phytoplankton Pigments in Oceanography: Guidelines to Modern Methods, 2nd edition, UNESCO Publishing, Paris, 2005.
[27] D. Bína, Z. Gardian, M. Herbstová, R. Litvín, Modular antenna of photosystem I in secondary plastids of red algal origin: a *Nannochloropsis oceanica* case study, Photosynth. Res. 131 (2017) 255–266.
[28] A. Zouni, J. Kern, J. Frank, T. Hellweg, J. Behlke, W. Saenger, K.-D. Irrgang, Size determination of cyanobacterial and higher plant photosystem II by gel permeation chromatography, light scattering, and ultracentrifugation, Biochemistry 44 (2005) 4572–4581.
[29] W. Kühlbrandt, D.N. Wang, Y. Fujiyoshi, Atomic model of plant light-harvesting complex by electron crystallography, Nature 367 (1994) 614–621.
[30] S. Basso, D. Simionato, C. Gerotto, A. Segalla, G.M. Giacometti, T. Morosinotto, Characterization of the photosynthetic apparatus of the Eustigmatophycean *Nannochloropsis gaditana*: evidence of convergent evolution in the supramolecular organization of photosystem I, Biochim. Biophys. Acta 1837 (2014) 306–314.
[31] M.J. Llansola-Portoles, R. Litvín, C. Ilioaia, A.A. Pascal, D. Bína, B. Robert, Pigment structure in the violaxanthin–chlorophyll-a–binding protein VCP, Photosynth. Res. 134 (2017) 51–58.
[32] I. Moya, M. Silvestri, O. Vallon, G. Cinque, R. Bassi, Time-resolved fluorescence analysis of the photosystem II antenna proteins in detergent micelles and liposomes, Biochemistry 40 (2001) 12552–12561.
[33] Y. Miloslavina, A. Wehner, P.H. Lambrev, E. Wientjes, M. Reus, G. Garab, R. Croce, A.R. Holzwarth, Far-red fluorescence: a direct spectroscopic marker for LHCII oligomer formation in non-photochemical quenching, FEBS Lett. 582 (2008) 3625–3631.
[34] R. Croce, A. Chojnicka, T. Morosinotto, J.A. Ihalainen, F. van Mourik, J.P. Dekker, R. Bassi, R. van Grondelle, The low-energy forms of photosystem I light-harvesting complexes: spectroscopic properties and pigment-pigment interaction characteristics, Biophys. J. 93 (2007) 2418–2428.
[35] J.T.M. Kennis, A.M. Streltsov, S.I.E. Vulto, T.J. Aartsma, T. Nozawa, J. Amesz, Femtosecond dynamics in isolated LH2 complexes of various species of purple bacteria, J. Phys. Chem. B 101 (1997) 7827–7834.
[36] H.M. Visser, O.J.G. Somsen, F. van Mourik, Su Lin, I.H.M. van Stokkum, R. van Grondelle, Direct observation of sub-picosecond equilibration of excitation energy in the light-harvesting antenna of *Rhodospirillum rubrum*, Biophys. J. 69 (1995) 1083–1099.
[37] H. Cong, D.M. Niedzwiedzki, G.N. Gibson, H.A. Frank, Ultrafast time-resolved spectroscopy of xanthophylls at low temperature, J. Phys. Chem. B 112 (2008) 3558–3567.
[38] D.M. Niedzwiedzki, D.J. Sandberg, H. Cong, M.N. Sandberg, G.N. Gibson, R.R. Birge, H.A. Frank, Ultrafast time-resolved absorption spectroscopy of geometric isomers of carotenoids, Chem. Phys. 357 (2009) 4–16.
[39] G. Cerullo, D. Polli, G. Lanzani, S. De Silvestri, H. Hashimoto, R.J. Cogdell, Photosynthetic light harvesting by carotenoids: detection of an intermediate excited state, Science 298 (2002) 2395–2398.
[40] D.M. Niedzwiedzki, D. Bina, N. Picken, S. Honkanen, R.E. Blankenship, D. Holten, R.J. Cogdell, Spectroscopic studies of two spectral variants of light-harvesting complex 2 (LH2) from the photosynthetic purple sulfur bacterium *Allochromatium vinosum*, Biochim. Biophys. Acta 1817 (2012) 1576–1587.
[41] R. Croce, M.G. Müller, R. Bassi, A.R. Holzwarth, Carotenoid-to-chlorophyll energy transfer in recombinant major light-harvesting complex (LHCII) of higher plants. I. femtosecond transient absorption measurements, Biophys. J. 80 (2001) 901–915.
[42] W.P. Bricker, P.M. Shenai, A. Ghosh, Z. Liu, M.G.M. Enriquez, P.H. Lambrev, H.-S. Tan, C.S. Lo, S. Tretiak, S. Fernandez-Albertim, Y. Zhao, Non-radiative relaxation of photoexcited chlorophylls: theoretical and experimental study, Sci. Rep. 5 (2015) 13625.
[43] B. Gobets, R. van Grondelle, Energy transfer and trapping in photosystem I, Biochim. Biophys. Acta 1507 (2001) 80–99.
[44] J.A. Ihalainen, R. Croce, T. Morosinotto, I.H.M. van Stokkum, R. Bassi, J.P. Dekker, R. van Grondelle, Excitation decay pathways of Lhca proteins: a time-resolved fluorescence study, J. Phys. Chem. B 109 (2005) 21150–21158.
[45] F. Passarini, E. Wientjes, H. van Amerongen, R. Croce, Photosystem I light-harvesting complex Lhca4 adopts multiple conformations: red forms and excited-state quenching are mutually exclusive, Biochim. Biophys. Acta 1797 (2010) 501–508.
[46] D. Bína, K. Bouda, R. Litvín, A two-component nonphotochemical fluorescence quenching in eustigmatophyte algae, Photosynth. Res. 131 (2017) 65–77.
[47] Z. Kvíčalová, J. Alster, E. Hofmann, P. Khoroshyy, R. Litvín, D. Bína, T. Polívka, J. Pšenčík, Triplet–triplet energy transfer from chlorophylls to carotenoids in two antenna complexes from dinoflagellate *Amphidinium carterae*, Biochim. Biophys. Acta 1857 (2016) 341–349.
[48] P. Khoroshyy, D. Bína, Z. Gardian, R. Litvín, J. Alster, J. Pšenčík, Quenching of chlorophyll triplet states by carotenoids in algal light-harvesting complexes related to fucoxanthin-chlorophyll protein, Photosynth. Res. 135 (2018) 213–225.
[49] D. Carbonera, A. Agostini, M. Di Valentin, C. Gerotto, S. Basso, G.M. Giacometti, T. Morosinotto, Photoprotective sites in the violaxanthin–chlorophyll a binding protein (VCP) from *Nannochloropsis gaditana*, Biochim. Biophys. Acta 1837 (2014) 1235–1246.
[50] A. Gelzinis, J. Chmeliov, A.V. Ruban, L. Valkunas, Can red-emitting state be responsible for fluorescence quenching in LHCII aggregates? Photosynth. Res. 135 (2018) 275–284.